ACS Catalysis

Research Article

pubs.acs.org/acscatalysis

Mechanistic Studies on Stereoselective Organocatalytic Direct β-C−H Activation in an Aliphatic Chain by Chiral N-Heterocyclic Carbenes

Yernaidu Reddi and Raghavan B. Sunoj*

Department of Chemistry, Indian Institute of Technology Bombay, Powai, Mumbai 400076, India

Supporting Information

ABSTRACT: The functionalization of aliphatic and aromatic C−H bonds has remained a priority in transition-metal catalysis for the last few decades. N-heterocyclic carbenes (NHCs) have very recently been proven as an effective organocatalytic alternative toward site-selective sp^3 β-C−H bond functionalization in aliphatic esters and related compounds. We have employed modern density functional theory computations to provide the first mechanistic insights into this entirely new form of reactivity of NHCs, leading to β-C−H bond activation. NHC-catalyzed coupling between hydrazone and β-phenyl propionate leading to a γ-lactam bearing two chiral centers is reported. An interesting two-step mechanistic cascade that helps surmount the high bond dissociation energy of an otherwise inert β-C−H bond is identified. An initial addition−elimination at the ester group installs the chiral triazolium NHC to the substrate. The deprotonation of the α-C−H by the departing phenoxide first furnishes an α-enolate intermediate. A concerted protonation at the enolate oxygen by the phenol and a β-C−H deprotonation by the phenoxide leads to the vital nucleophilic β-carbanion intermediate. The origin of enantioselectivity in the C−C bond formation between the *si* prochiral face of the nucleophilic β-carbon and the *re* face of electrophilic hydrazone is traced to the differential in the C−H···π, C−H···O, and N−H···O interactions that exist in the transition states for the lower energy *si*,*re* and higher energy *re*,*si* modes in the Michael addition step. The computed enatio- and diastereoselectivities are in very good agreement with those in an earlier experimental report.

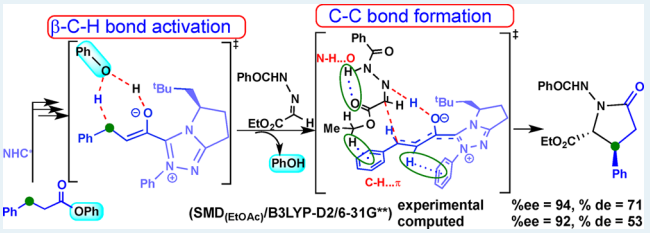

KEYWORDS: *N-heterocyclic carbenes, C−H bond functionalization, stereoselectivity, reaction mechanism, transition states, density functional theory*

INTRODUCTION

Significant efforts have been expended in recent years toward developing methodologies for the selective functionalization of inert C−H bonds. While α-C−H bond functionalization has become a straightforward task, the inertness of β- as well as γ-C−H bonds poses formidable challenges.[1] The most recent trends, however, indicate three emerging protocols to accomplish β-C−H bond functionalization of alkyl chains. These include catalytic methods using (a) transition metals in conjunction with suitably placed directing groups on the substrates,[2] (b) photoredox approaches,[3] and (c) N-heterocyclic carbenes (NHCs).[4] An illustration of these key approaches is provided in Scheme 1, by using a select set of examples. All of these methodological advances hold promise in selective functionalization and have enabled access to relative complex synthetic targets as well. Among these protocols, NHC catalysis stands out as a unique organocatalytic approach to C−H bond functionalization.

Organocatalysis has become a widely employed strategy toward the synthesis of complex natural products from relatively simpler precursors such as aldehydes, ketones, and esters.[5] N-heterocyclic carbenes (NHCs) have made a mark as effective organocatalysts, particularly in the development of new asymmetric transformations. While the inception and early acceptance of NHCs have remained rather slow,[6] a recent renaissance has provided the right impetus to the domain of NHC catalysis to come to the forefront of chemical catalysis.[7] Pioneering contributions from the groups of Berkessel, Bode, Chi, Enders, Glorius, Lupton, Nair, Rovis, Scheidt, and others have helped in realizing the potential of NHCs as powerful catalysts in asymmetric synthesis.[8] In most of the NHC-catalyzed reactions, the two vital features of NHCs are suitably harnessed. These are the ability of NHCs to (a) impart an umpolung-type reactivity to an otherwise electrophilic functional group such as an aldehyde and (b) render homoenolate attributes to conjugated aldehydes such as an enal.[1f,5i,7,8b]

Another recent discovery that expanded the scope of NHC catalysis came from the Chi group in the form of sp^3 β-C−H bond activation in saturated carboxylic esters.[4b,9] This strategy, which has also been successfully extended by using chiral NHCs, is proposed to involve the generation of a nucleophilic reactive center at the β carbon. The reactivity of a nucleophilic β carbon has been demonstrated with a range of electrophiles such as enones, trifluoro ketones, and hydrazones with high stereoselectivity.[9] One of the most recent illustrations of a β-

Received: August 23, 2015
Published: August 26, 2015

DOI: 10.1021/acscatal.5b01870
ACS Catal. 2015, 5, 5794−5802

Scheme 1. Selected Set of Recent Examples of β-C−H Bond Functionalization of Saturated Carbonyl Compounds using Different Catalytic Approaches

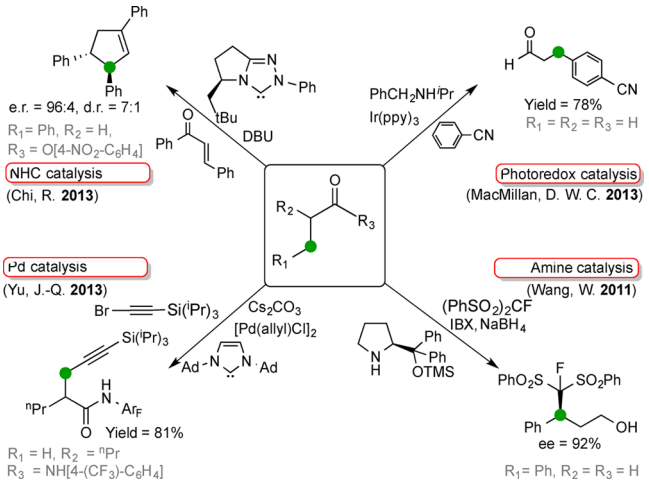

C−H functionalization by using a chiral NHC is provided in Scheme 2. This method provides an elegant access to highly functionalized γ-lactams. It is important to note that some of the γ-lactams can be suitably converted to pharmaceutically significant compounds such as Balcofen and Rolipram, which are respectively used in the treatment of spasticity and as a potent phosphodiesterase inhibitor.[9]

Scheme 2. Chiral NHC-Catalyzed Asymmetric β-C−H Functionalization of a Saturated Carboxylic Ester

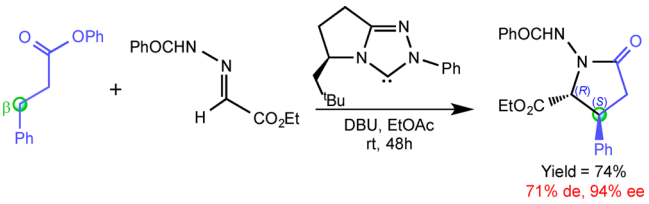

A few important features of the above reaction are noteworthy. Although sp^3 C−H bonds farther from an electron-withdrawing substituent generally exhibit high bond dissociation energies, the functionalization of the β-C−H bond in this reaction could be performed under mild and ambient conditions by using NHC catalysis. More importantly, high enantio- and diastereoselectivities in the formation of γ-lactam could be accomplished by using a relatively simpler chiral NHC bearing just one chiral center. A closer perusal of the current literature suggests that mechanistic investigations are certainly not commensurate with the rapid developments in NHC-catalyzed reactions. Although there have been computational studies focusing on homoenolate as well as umpolung type NHC catalysis,[10] no reports have been available to date on the mechanism of this new form of NHC reactivity leading to β-C−H functionalization. As part of our continued efforts in gaining mechanistic insights into NHC-catalyzed reactions,[10a,b,f,g,i] we became interested in probing this asymmetric NHC-catalyzed β-C−H functionalization reaction by using density functional theory computational methods. In particular, we intend to disclose (a) the energetic features of the most preferred pathway responsible for the formation of a chiral γ-lactam product via a β-C−H activation route, (b) the nature of the key intermediates and the transition states, and (c) the origin of stereoselectivity imparted by the chiral NHC catalyst.

Scheme 3. Key Mechanistic Steps Involved in β-C−H Activation of Saturated Carboxylic Esters Catalyzed by NHCs

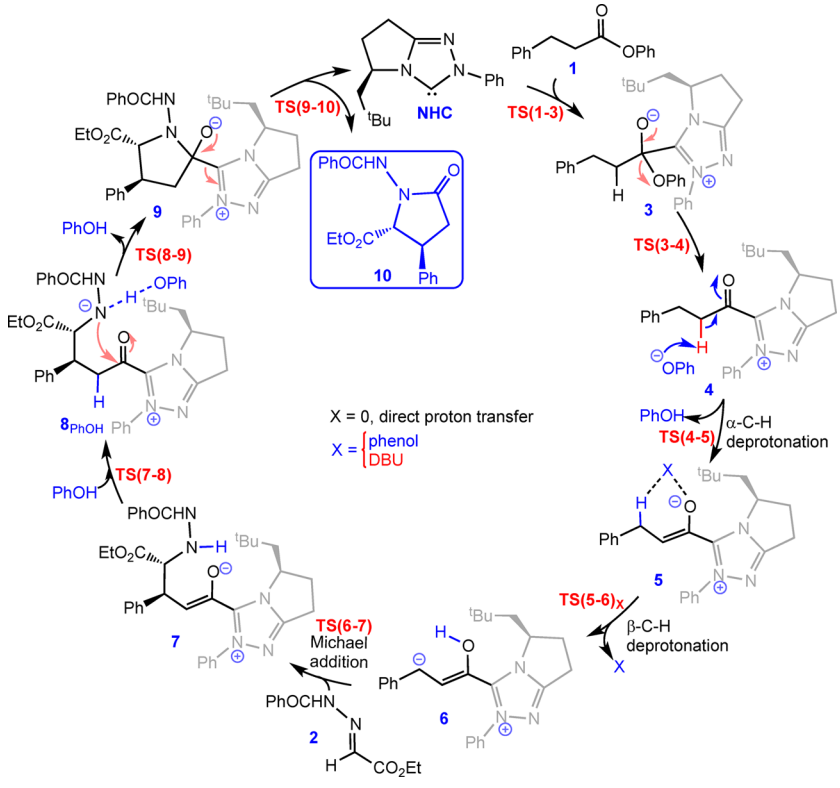

DOI: 10.1021/acscatal.5b01870
ACS Catal. 2015, 5, 5794−5802

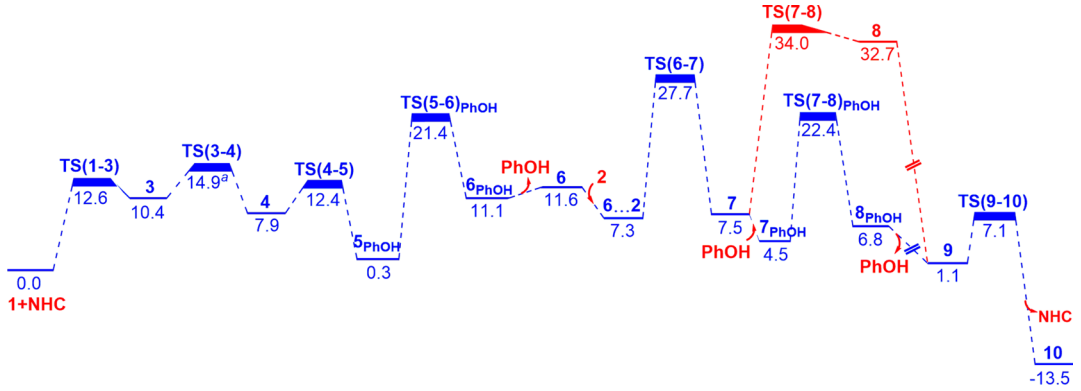

Figure 1. Gibbs free energy profile (in kcal/mol) for NHC-catalyzed direct β-C−H activation of a saturated carboxylic ester leading to the formation of γ-lactam obtained at the SMD_{EtOAc}/B3LYP-D2/6-31G** level. The Gibbs free energy value only for **TS(3-4)** is at the SMD_{EtOAc}/B3LYP-D2/6-31G**//B3LYP-D2/6-31G** level of theory.[28] The pathway shown in red represents a higher energy alternative without the involvement of a explicit phenol.

COMPUTATIONAL METHODS

DFT (density functional theory) calculations on all of the stationary points such as intermediates, reactants, and transition states were carried out using the B3LYP-D2[11] and M06-2X[12] functionals in conjunction with the 6-31G** basis set. The B3LYP-D3[13] and B3LYP[14] computations were also performed only for the stereoselective C−C bond formation step. The fully optimized geometries of all stationary points were characterized by frequency calculations in order to verify that (a) the transition states have one and only one imaginary frequency pertaining to the desired reaction coordinate and (b) all minimum energy structures have only a positive Hessian index. In addition, the thermal and entropic corrections obtained through the frequency calculations are included toward obtaining the Gibbs free energies of all the stationary points. The intrinsic reaction coordinate (IRC) calculations developed by Schlegel[15] were performed at the B3LYP-D2 and M06-2X levels of theory to further authenticate that the transition states on the energy profiles connect to the desired minima on either side of the first-order saddle point. The enthalpies and Gibbs free energies in the gas phase for all stationary points were obtained by adding the zero-point vibrational energy (ZPVE) and thermal energy corrections obtained by using standard statistical mechanics approximations at 298.15 K and 1 atm of pressure. All calculations were carried out using the Gaussian09 suite of quantum chemical programs.[16]

The effect of continuum solvation was incorporated by using the SMD solvation model, wherein the full solute electron density is employed without defining partial atomic charges.[17] Since the experimental studies employed ethyl ethanoate (EtOAc) as a solvent, we have employed the continuum dielectric of EtOAc (ε = 5.9867). The Gibbs free energies and enthalpies for all stationary points in the condensed phase were computed by adding the corresponding thermal and entropic corrections obtained in the gas phase to the single-point energies in the solvent continuum. The full geometry optimizations in the condensed phase were also carried out at the SMD_{EtOAc}/B3LYP-D2/6-31G** level of theory for the stereoselectivity step for the 4 lowest energy stereocontrolling transition states out of 32 conformations/configurations examined in the gas phase. Topological analysis of the electron densities using the atoms-in-molecules (AIM) formalism was carried out by using AIM2000 software.[18] The activation−strain analysis was carried out to probe the origin of the energy difference between the stereocontrolling transition states in greater detail.[19] Natural bonding orbital (NBO) analysis[20] on some of the intermediates was performed to analyze the natural charges as well as to obtain the Wiberg bond indices.

RESULTS AND DISCUSSION

The broad features of the mechanism involved in NHC-catalyzed direct β-C−H activation of saturated carboxylic esters leading to the formation of γ-lactams can be gathered from Scheme 3. The description herein focuses on the most preferred pathway identified on the basis of the computed Gibbs free energies at the SMD_{EtOAc}/B3LYP-D2/6-31G** level of theory. Alternative mechanistic pathways as well as conformational possibilities are provided in the Supporting Information. In the initial step, the nucleophilic NHC adds to the carbonyl carbon of the ester to form the zwitterionic NHC ester intermediate **3**. This being an addition−elimination step, the phenoxide tends to leave the intermediate, in the forward direction of the transition state.[21] However, an ion-pair intermediate (**4**) appears to be a more likely scenario, wherein the phenoxide develops multiple hydrogen-bonding interactions with the α hydrogen (2.03 Å), *N*-phenyl hydrogen (1.96 Å), and the phenyl hydrogen of the β-carbon (2.38 Å) (see Figure S2 in the Supporting Information). In the ensuing step, the phenoxide abstracts the acidic α-C−H proton to form the enolate intermediate **5**.[22] On the other hand, if the phenoxide abstracts the β-C−H proton, it can give rise to formation of another β-carbanion intermediate. However, the activation barrier associated with this pathway is more than 22 kcal/mol higher than the α-C−H deprotonation.[23] The β-C−H protons of intermediate **5** are expected to be more acidic, due to an extended conjugation of the resulting carbanionic species with the triazolium moiety.[24] There are two key possible avenues that enolate intermediate **5** can be envisaged to proceed. A deprotonation of the β-C−H proton can generate intermediate **6** having a nucleophilic center at the β-carbon. Alternatively, **5** can be intercepted by the electrophile hydrazone (**2**) present in the reaction medium. However, this pathway is found to be significantly higher in energy than the deprotonation process leading to **6**. Furthermore, the product arising from such a pathway has not been observed under the experimental conditions.[25]

DOI: 10.1021/acscatal.5b01870
ACS Catal. 2015, 5, 5794−5802

In one of the most important steps in this catalytic cycle, Michael addition of intermediate **6** to electrophilic hydrazone takes place. The resulting Michael adduct **7** has two new stereocenters that are retained through the final product. Hence, the decision of what would be the preferred enantiomer and diastereomer in the reaction is made at this stage. It is noticed that the stereocontrolling C−C bond formation is accompanied by a concomitant abstraction of the enol proton by the hydrazone nitrogen (vide infra, Figure 4). The proton transfer back from the hydrazone nitrogen to the nucleophilic α-carbon of the enolate in **7** helps in the generation of intermediate **8**. Subsequent lactamization leads to intermediate **9**, which upon expulsion of the NHC yields the γ-lactam product with two chiral centers.

The computed Gibbs free energies of the lowest energy intermediates and the transition states involved in the formation of γ-lactam are presented in the form of an energy profile diagram in Figure 1. Some of the vital features of the energy profile for the most preferred pathway and a comparison with alternative higher energy possibilities are discussed here. In the first step, the chiral NHC adds to ester carbonyl group via **TS(1-3)** to give the zwitterionic intermediate **3**, with an activation barrier of 12.6 kcal/mol.[26] The expulsion of the phenoxide is noted to be quite feasible, as revealed by the relative energy of **TS(3-4)**. The intermediate thus formed (**4**) can provide the enolate **5**, when the departing phenoxide abstracts the proton from the most acidic α-proton of the ester. The relative energy of the proton abstraction transition state (**TS(4-5)**) is 12.4 kcal/mol, and the corresponding elementary step barrier is 4.5 kcal/mol. Since a large excess of DBU is employed in this reaction,[9] we have examined another possibility wherein DBU abstracts the α-proton from the initially formed zwitterionic intermediate (**3**), thereby creating a direct route for **3** to **5** conversion. Subsequently, the departing phenoxide can abstract the proton from the protonated DBU. The relative energy of $\mathbf{TS(3\text{-}5)}_{\mathbf{DBU}}$ in this direct E2 elimination pathway is found to be as high as 26.8 kcal/mol, which is evidently higher than the stepwise process (i.e., **3** to **5** via **4**).[27] It is therefore evident that the kinetically preferred pathway proceeds through **TS(4-5)**. In addition, the exoergicity for **4** + DBU → **5** + [DBU−$H^{+}\cdots{}^{-}$OPh] is found to be −5.8 kcal/mol, suggesting that the participation of DBU provides an additional thermodynamic drive in this step of the reaction.

The most important step in this catalytic cycle is β-C−H activation, leading to the nucleophilic intermediate **6**. The formation of **6** requires that the β-C−H proton is transferred to the enolate oxygen. This deprotonation could proceed via three likely pathways, such as an unassisted direct proton transfer or a DBU-assisted or phenol-assisted proton transfer. Such assisted proton transfers can be regarded as a reasonable route in view of the use of excess DBU in the reaction as well as the fact that a molecule of phenol is released in an earlier step involved in the formation the α-enolate intermediate (**5**). A direct transfer of the β-C−H proton to the enolate oxygen through a five-membered transition state geometry **TS(5-6)**, as shown in Figure 2, is found to be about 37 kcal/mol. However, relative Gibbs free energies of $\mathbf{TS(5\text{-}6)}_{\mathbf{DBU}}$ and $\mathbf{TS(5\text{-}6)}_{\mathbf{PhOH}}$ for the DBU- and phenol-assisted proton transfers are respectively 29.7 and 21.4 kcal/mol. The analysis of the geometric features of $\mathbf{TS(5\text{-}6)}_{\mathbf{PhOH}}$ and extended intrinsic reaction coordinate (IRC) calculations reveal a concerted protonation−deprotonation transition state.[29] An early protonation of the enolate oxygen and a concomitant abstraction of a proton from the sp^3 β-carbon by the developing phenoxide are noticed.[30] It is therefore highly likely that a phenol-assisted β-C−H activation is the most preferred route for the formation of the β-carbanion intermediate **6**. It is also important to note that the presence of an aryl group is vital to the generation of β-carbanion **6**. To examine whether the β-substituent plays any major role in deciding the course of this reaction, we have replaced the aryl group with a methyl group at the β-carbon. The relative Gibbs free energy of the deprotonation transition state is found to be 5.5 kcal/mol higher for the β-methyl in comparison to the β-phenyl in the phenol-assisted β-C−H activation mode. Building on this, a Hammett correlation for this step of the catalytic cycle with a range of para substituents revealed a preference toward electron-withdrawing substituents at the para position of the β-phenyl substituent (vide infra).

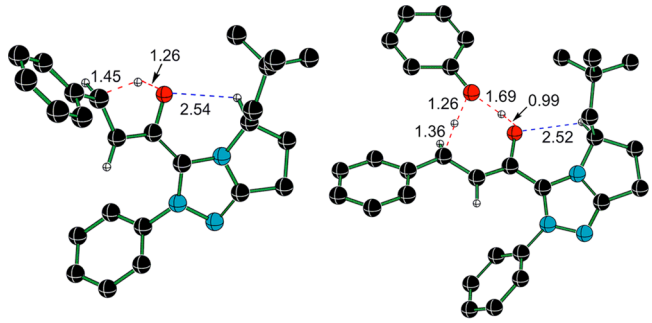

TS(5-6) (37.0) $\mathbf{TS(5\text{-}6)}_{\mathbf{PhOH}}$ (21.4)

Figure 2. Optimized geometries for β-C−H activation through unassisted and phenol-assisted transition states obtained at the SMD_{EtOAc}/B3LYP-D2/6-31G** level of theory. The bond lengths are given in Å. The relative Gibbs free energies with respect to the infinitely separated reactants given in parentheses are in kcal/mol. Only selected hydrogens are shown for improved clarity. Atom color code: black, C; ivory, H; cyan, N; red, O.

The nucleophilic β-carbon in intermediate **6** gives it Michael donor characteristics. Michael addition with electrophilic hydrazone leads to the formation of a new C−C bond. It is noted that in **TS(6-7)** the C−C bond formation is accompanied by a concerted proton transfer from the enol oxygen to the hydrazone nitrogen to give intermediate **7**.[31] Since both nucleophile and electrophile offer prochiral faces, several stereochemically distinct modes of C−C bond formation leading to two new chiral carbon centers can be envisaged. In addition to such configurational features, there would also be a larger number of conformational possibilities. To identify the most preferred C−C bond formation transition state, an exhaustive sampling encompassing 32 conformational and configurational possibilities has been carried out. Three important dihedral angles, as shown in Figure 3a, were varied, and the corresponding transition states were then optimized. The dihedral angles Φ_1(N1−C2−C3−O4), Φ_2(C5−C6−C7−N8), and Φ_3(N8−N9−C10−O11) captures the critical region of the conformational space, including that along the reaction coordinate. In addition, the positioning of the *N*-phenyl group of the chiral catalyst, either nearer to or farther from the enolate oxygen, is considered as well. All of these possibilities have been examined for the addition of *re* or *si* prochiral faces of nucleophilic β-carbon on the prochiral faces of the hydrazone carbon. All 32 transition state possibilities for the stereo-controlling C−C bond formation, corresponding energies, and

DOI: 10.1021/acscatal.5b01870
ACS Catal. 2015, 5, 5794−5802

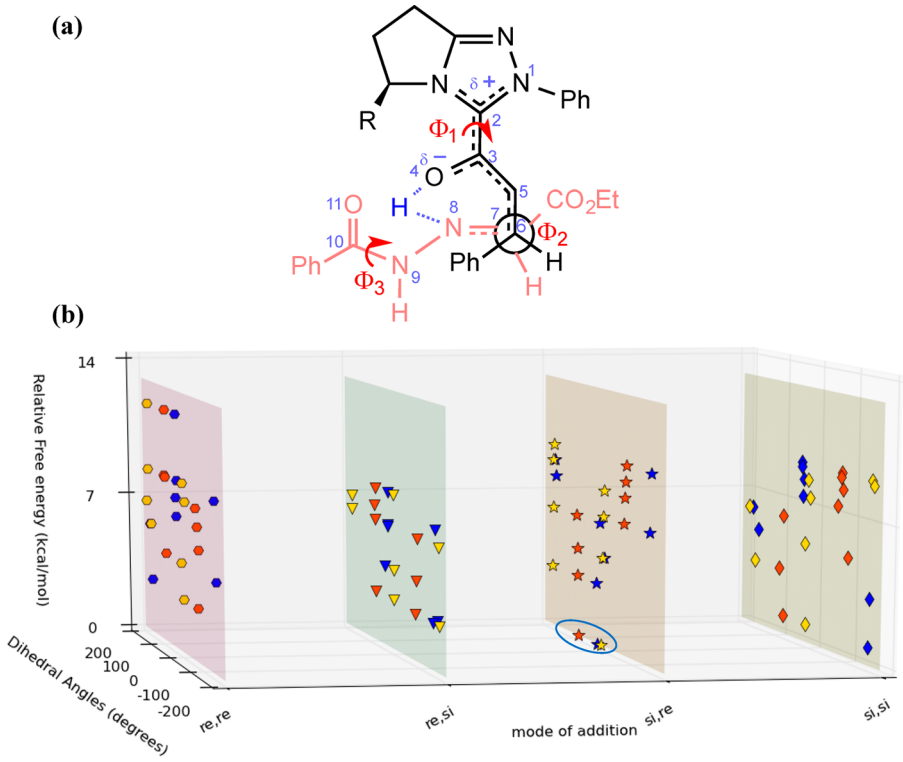

Figure 3. Correlation between the relative Gibbs free energies of the stereocontrolling C−C bond formation transition states and the key dihedral angles (Φ_1 (blue), Φ_2 (orange), and Φ_3 (yellow)) for the four stereochemically distinct modes of addition of the nucleophilic β-carbon on hydrazone: (a) important dihedral angles (Φ_1, Φ_2, and Φ_3) used in the conformational sampling; (b) summary of Gibbs free energy distribution across different conformations and configurations of the C−C bond formation transition states.The lowest energy TS inscribed belongs to the **TS(6-7)**$_{si,re}$ mode of addition.

optimized geometries are provided in Table S3 and Figures S11 and S12 in the Supporting Information.

A succinct representation of the energy distribution of the stereocontrolling transition states as a function of the mode of addition and other conformational parameters is provided in Figure 3b. A quick inspection of these data reveals certain interesting general features of these transition states. Some of the lowest energy transition states can be found on the two of the rightmost vertical plates that correspond to the **TS(6-7)**$_{si,re}$ and **TS(6-7)**$_{si,si}$ modes of addition of the nucleophilic β-carbon to the hydrazone carbon. It can be further noted that the addition through the *si* prochiral face of the β-carbon is distinctly more preferred over that through its *re* face. The lowest energy stereocontrolling transition state for the C−C bond formation exhibits a dihedral angle Φ_1, Φ_2, Φ_3 combination of 14.8, 81.2, 4.6°. Such a mode of addition results in a 2*R*,3*S* product configuration, which is in agreement with the experimental observation. The difference in Gibbs free energies between the diastereomeric transition states **TS(6-7)**$_{si,re}$ and **TS(6-7)**$_{re,si}$, which is responsible for enantioselectivity, is found to be 1.9 kcal/mol. This energy separation corresponds to 92% ee, which is in excellent agreement with the experimentally reported value of 94%.[9] Similarly, the diastereoselectivity computed on the basis of the difference in Gibbs free energies between **TS(6-7)**$_{si,re}$ and **TS(6-7)**$_{si,si}$ is 53% de, which is in concert with the experimental value (71%).[9] The energy differences between the stereocontrolling transition states obtained using different functionals such as B3LYP-D3 (L3), M06-2X (L4), and B3LYP (L5) all convey the same trends (Figure 4). With all of these functionals, the energetic order of preference for different stereochemical modes of addition of the nucleophile to the electrophile is *si,re* < *si,si* < *re,si* < *re,re*.

After having identified the enantio- and diastereocontrolling transition states, we turned our attention to the stereoelectronic factors that contribute to the differential stabilization. As a first step in this direction, the optimized geometries of the C−C bond formation transition states have been carefully analyzed. The three key geometric parameters *a*, *b*, and *c* respectively represent the bond distances of the incipient C−C bond and those associated with the transfer of the enol proton to the hydrazone nitrogen (Figure 4).[32] A fairly large number of noncovalent interactions, such as C−H···π, C−H···O, C−H···N, and N−H···O, are identified. These interactions are depicted in Figure 4 as follows; C−H···π (*e* and *m*), C−H···O (*d*, *g*−*i*, *k*, and *l*), C−H···N (*f*), and N−H···O (*j*).[33] Additional analyses toward identifying the existence of these interactions were done by using the atoms-in-molecules (AIM) formalism. The topological distribution of the electron density revealed the presence of bond paths connecting the interacting atoms, and the corresponding electron densities at the bond critical points are noted.[34]

As shown in Figure 4, x1 and x2 are centroids of two phenyl rings.[35] C−H···π interactions are identified in the stereocontrolling C−C bond formation transition states on the basis of the above parameters. The efficiencies of the C−H···π interaction (*e*) in both of the lower energy diastereomeric transition states **TS(6-7)**$_{si,re}$ and **TS(6-7)**$_{re,si}$ are found to be similar. Interestingly, an additional C−H···π interaction (between the β-phenyl ring and the methylene hydrogen of the ethyl ester of the hydrazone moiety (m = 2.60 Å and θ_2 = 35.9°)) is present in the lowest energy transition state **TS(6-**

DOI: 10.1021/acscatal.5b01870
ACS Catal. 2015, 5, 5794−5802

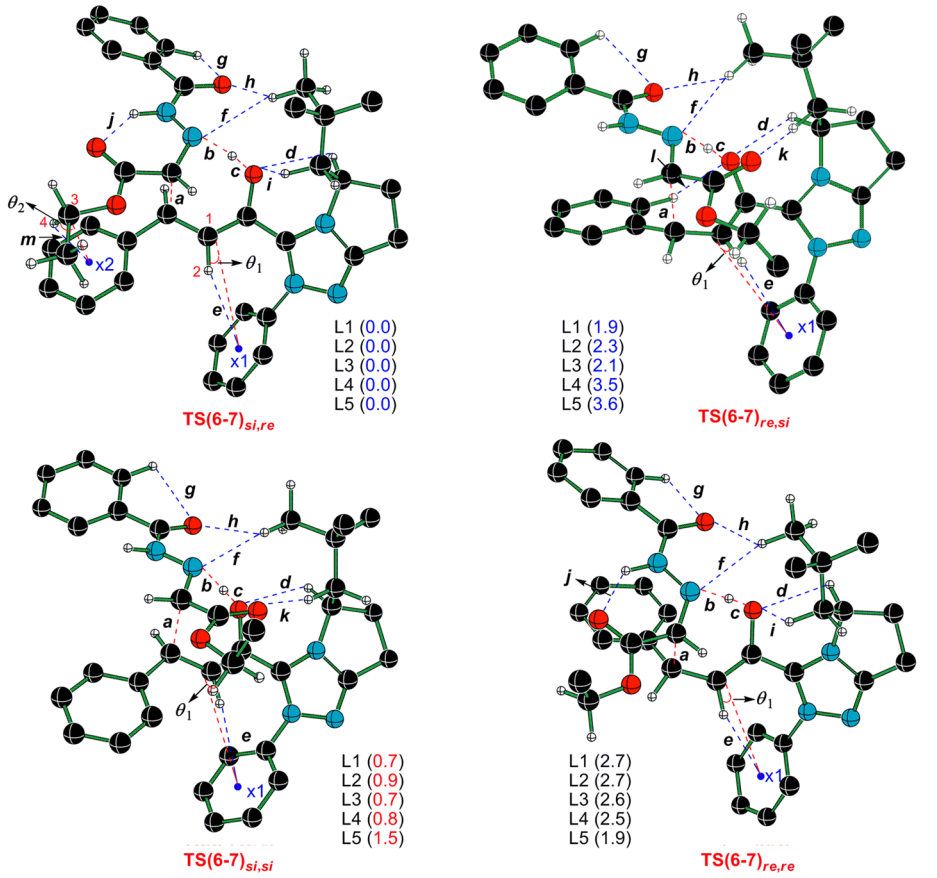

TS(6-7)	a	b	c	d	e	f	g	h	i	j	k	l	m	θ_1	θ_2
si,re	1.95	1.65	1.02	2.53	2.97	2.74	2.49	2.48	2.51	1.97	–	–	2.60	32.6	35.9
re,si	2.01	1.68	1.01	2.47	2.92	2.60	2.50	2.75	–	–	2.36	2.26	–	32.2	–
si,si	1.97	1.66	1.01	2.49	2.87	2.51	2.52	2.91	–	–	2.36	–	–	30.4	–
re,re	1.99	1.65	1.02	2.52	3.11	2.64	2.49	2.54	2.52	1.98	–	–	–	38.2	–

Figure 4. Optimized geometries of the stereocontrolling C−C bond formation transition states at the SMD_{EtOAc}/B3LYP-D2/6-31G** level of theory: L1, SMD_{EtOAc}/B3LYP-D2/6-31G**; L2, SMD_{EtOAc}/B3LYP-D2/6-31G**//B3LYP-D2/6-31G**; L3, SMD_{EtOAc}/B3LYP-D3/6-31G**//B3LYP-D3/6-31G**; L4, SMD_{EtOAc}/M06-2X/6-31G**//M06-2X/6-31G**; L5, SMD_{EtOAc}/B3LYP/6-31G**//B3LYP/6-31G**. The bond lengths and angles are in Å and deg, respectively. Only selected hydrogens are shown for improved clarity.

TS(6-7)$_{si,re}$, which is absent in the higher energy **TS(6-7)**$_{re,si}$. Other stabilizing contacts, namely the C−H···O interactions (*d* and *g*), are found to be nearly identical in both **TS(6-7)**$_{si,re}$ and **TS(6-7)**$_{re,si}$. However, the C−H···O interaction between the carbonyl oxygen of the hydrazone moiety and the *tert*-butyl group on the NHC (*h*) in **TS(6-7)**$_{si,re}$ is shorter (2.48 Å) than that in the **TS(6-7)**$_{re,si}$ (2.75 Å) mode. In addition, a fairly strong N−H···O interaction (*j*) that is present in the **TS(6-7)**$_{si,re}$ transition state (1.97 Å) is absent in the **TS(6-7)**$_{re,si}$ mode. The cumulative effect of the relative efficiencies of all these interactions gives rise to the vital energy difference of 1.9 kcal/mol between the diastereomeric transition states **TS(6-7)**$_{si,re}$ and **TS(6-7)**$_{re,si}$.[36] The computed enantioselectivity of 92% is in very good agreement with the experimental value of 94%. It is interesting to note that the nucleophilic *β*-carbon approaches the electrophilic hydrazone from the same side of the *tert*-butyl substituent at the chiral center of the NHC. The use of a qualitative transition state model that generally relies on steric interactions would have promoted this approach. However, quantitative insights into the type and nature of the weak stabilizing interactions helped us locate a large number of lower energy transition states, as presented in this section. More importantly, when the electrophile approaches from the face opposite to that of the *tert*-butyl group, the number of weak interactions is found to be less effective and thus results in higher energy transition states.[37]

The relative Gibbs free energy for stereoselective C−C bond formation via **TS(6-7)** is found to be 27.7 kcal/mol in the most preferred mode of addition (Figure 1). The resulting enolate intermediate **7** undergoes a proton transfer from the hydrazone N−H to the nucleophilic *α*-carbon, leading to intermediate **8**. The relative Gibbs free energy of **TS(7-8)** is 34.0 kcal/mol for the formation of intermediate **8** (Figure 1). Since a large excess of DBU is used in the reaction,[9] it might assist as well in this proton transfer. Hence, we have examined an alternative possibility wherein DBU abstracts the proton from the hydrazone nitrogen first to form a protonated DBU, which then transfers the proton to the *α*-carbon to give intermediate **8**. The relative Gibbs free energy of the transition state **TS(7-8)**$_{DBU}$ for the proton transfer is found to be even higher (37.5

DOI: 10.1021/acscatal.5b01870
ACS Catal. 2015, 5, 5794−5802

kcal/mol) than that of an unassisted proton transfer via **TS(7-8)**. The relative Gibbs free energy of intermediate **8** is also found be rather high (32.7 kcal/mol) due to the negatively charged hydrazone nitrogen. In view of these features, we have included an explicit molecule of phenol (which gets generated in the course of the reaction, vide supra) as a hydrogen-bond donor to the hydrazone nitrogen. The inclusion of phenol stabilizes both the transition state (**TS(7-8)**) as well as the intermediate (**8**). The relative Gibbs free energy of this refined transition state, $\mathbf{TS(7\text{-}8)}_{\mathbf{PhOH}}$, for the proton transfer is 22.4 kcal/mol, which is lower than those of the unassisted and the DBU-assisted proton transfer transition states. The optimized geometries for the unassisted and phenol-bound five-membered proton transfer transition states are shown in Figure 5.

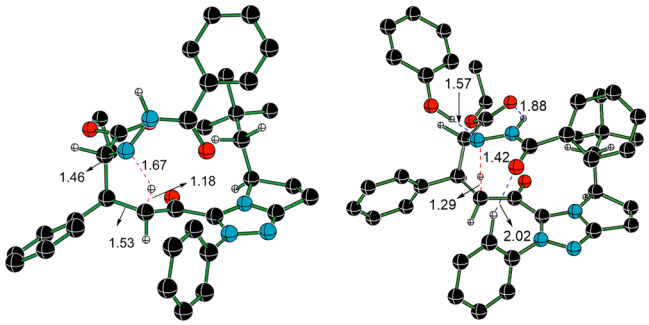

TS(7-8) (34.0) $\mathbf{TS(7\text{-}8)}_{\mathbf{PhOH}}$ (22.4)

Figure 5. Optimized geometries of transition states for the five-membered proton transfer step at the SMD_{EtOAc}/B3LYP-D2/6-31G** level of theory. The bond lengths are given in Å. Only selected hydrogens are shown for improved clarity. The relative Gibbs free energies, with respect to the infinitely separated reactants, are given in parentheses in kcal/mol.

Intermediate **8** can undergo an intramolecular lactamization to yield the γ-lactam intermediate **9** via **TS(8-9)**.[38] In the final step, the regeneration of NHC and release of γ-lactam occurs through the lower energy state **TS(9-10)** (Figure 1). The formation of γ-lactam product with a 2*S*,3*R* configuration is found to be exergonic by 13.5 kcal/mol. After having examined each elementary step leading to the final product, we have decided to examine the role of different aryl substituents on the energetics of the key steps involved in this reaction. Since the substrate is β-phenyl propionate, two kinds of substitution patterns have been considered: one on the ester −OAr group and the other on the β-phenyl group. The generalization of the key findings is provided herein in the form of Hammett analysis.

The difference in Gibbs free energies of the transition states, with (G_X) and without (G_H) a para substituent, has been plotted against the substituent constants (σ). A range of electron-donating and electron-withdrawing substituents is considered. Hammett correlations for β-C−H activation (**TS(5-6)**), C−C bond formation ($\mathbf{TS(6\text{-}7)}_{si,re}$), and intramolecular proton transfer (**TS(7-8)**) have yielded a positive reaction constant (ρ).[39] This indicates an accumulation of negative charge at the reaction center in the respective transition states. An overall rate enhancement could therefore be accomplished by introducing electron-withdrawing substituents on the aryl groups. These insights could be exploited by making a suitable choice of the substrate, or modifications therein, for improved β-C−H activation efficiency as well as the subsequent reaction with a given electrophile.

CONCLUSION

Mechanistic investigations on a chiral NHC-catalyzed direct β-C−H bond activation of an aliphatic carboxylic ester have been carried out by using the SMD_{EtOAc}/B3LYP-D2/6-31G** density functional theory computations in the solvent phase. The reaction involves a chiral NHC-catalyzed coupling between hydrazone and β-phenyl propionate leading to a γ-lactam as the final product with two chiral centers. In the initial addition−elimination step, the chiral NHC adds to the ester carbonyl, which is followed by the expulsion of the phenoxide. The α-C−H deprotonation in the resulting ketonic intermediate is facilitated by the departing phenoxide, rather than an external base (DBU) as described in the earlier working hypothesis. A more important role of the departing phenol is identified in the vital β-C−H activation step, where it helps in the transfer of proton from the β-carbon to the enolate oxygen. Again, the phenol-assisted pathway is noted as more favored over equivalent DBU-assisted and direct proton transfer alternatives. The role of a relative excess of DBU in the reaction could therefore be attributed to its participation in (a) generating the NHC from the corresponding triazolium precatalyst, (b) neutralizing the weakly acidic phenol that is released in the initial addition−elimination step, and (c) providing an additional thermodynamic impetus in the generation of α-enolate by forming an adduct with the departing phenol.

Even though participation of an α-enolate intermediate has been invoked in the catalytic cycle, the most favored pathway is found to be that wherein this α-enolate converts to a β-carbanion intermediate rather than directly reacting with the available electrophile (hydrazone). The barrier for the C−C bond formation reaction between the α-enolate and hydrazone is 2.5 kcal/mol higher in comparison to its conversion to β-carbanion, indicating a moderate kinetic advantage for the formation of th β-carbanion intermediate. Furthermore, no α-enolate products were noted under the experimental conditions. The intermolecular Michael addition of the *si* prochiral face of the nucleophilic β-carbon to the *re* face of electrophilic hydrazone is found to be the most preferred transition state for C−C bond formation. The enantiomeric and diastereomeric excesses of the γ-lactam (% ee 92, % de 53), computed on the basis of the Gibbs free energies of the stereocontrolling transition states, are in very good agreement with the experimental values (% ee 94, % de 71). The origin of enantioselectivity is traced to the differential C−H···π, C−H···O, and N−H···O interactions that exist in the stereocontrolling C−C bond formation transition states.

ASSOCIATED CONTENT

Supporting Information

The Supporting Information is available free of charge on the ACS Publications website at DOI: 10.1021/acscatal.5b01870.

Optimized geometries, description of mechanistic features, structural details of the transition states, and topological analysis of electron densities (PDF)

AUTHOR INFORMATION

Corresponding Author

*E-mail for R.B.S.: sunoj@chem.iitb.ac.in.

DOI: 10.1021/acscatal.5b01870
ACS Catal. 2015, 5, 5794−5802

Notes

The authors declare no competing financial interest.

■ ACKNOWLEDGMENTS

Y.R. acknowledges a senior research associate fellowship from IIT Bombay. The *SpaceTime* supercomputing facility at IIT Bombay is gratefully acknowledged for providing generous computing time.

■ REFERENCES

(1) (a) Chauhan, P.; Enders, D. *Angew. Chem., Int. Ed.* **2014**, *53*, 1485−1487. (b) Cheng, J.; Huang, Z.; Chi, Y. R. *Angew. Chem., Int. Ed.* **2013**, *52*, 8592−8596. (c) Xu, J.; Jin, Z.; Chi, Y. R. *Org. Lett.* **2013**, *15*, 5028−5031. (d) List, B.; Lerner, R. A.; Barbas, C. F., III *J. Am. Chem. Soc.* **2000**, *122*, 2395−2396. (e) Northrup, A. B.; MacMillan, D. W. C. *J. Am. Chem. Soc.* **2002**, *124*, 6798−6799. (f) Enders, D.; Niemeier, O.; Henseler, A. *Chem. Rev.* **2007**, *107*, 5606−5655. (g) Sohn, S. S.; Rosen, E. L.; Bode, J. W. *J. Am. Chem. Soc.* **2004**, *126*, 14370−14371. (h) Burstein, C.; Glorius, F. *Angew. Chem., Int. Ed.* **2004**, *43*, 6205−6208. (i) Mo, J.; Shen, L.; Chi, Y. R. *Angew. Chem., Int. Ed.* **2013**, *52*, 8588−8591. (j) Wang, D.-H.; Mei, T.-S.; Yu, J.-Q. *J. Am. Chem. Soc.* **2008**, *130*, 17676−17677. (k) Park, S. H.; Kim, J. Y.; Chang, S. *Org. Lett.* **2011**, *13*, 2372−2375. (l) Neisius, N. M.; Plietker, B. *Angew. Chem., Int. Ed.* **2009**, *48*, 5752−5755. (m) Chan, K. S. L.; Wasa, M.; Chu, L.; Laforteza, B. N.; Miura, M.; Yu, J.-Q. *Nat. Chem.* **2014**, *6*, 146−150. (n) Yang, W.; Ye, S.; Fanning, D.; Coon, T.; Schmidt, Y.; Krenitsky, P.; Stamos, D.; Yu, J.-Q. *Angew. Chem., Int. Ed.* **2015**, *54*, 2501−2504. (o) Deb, A.; Bag, S.; Kancherla, R.; Maiti, D. *J. Am. Chem. Soc.* **2014**, *136*, 13602−13605. (p) Modak, A.; Dutta, U.; Kancherla, R.; Maity, S.; Bhadra, M.; Mobin, S. M.; Maiti, D. *Org. Lett.* **2014**, *16*, 2602−2605. (q) Zhang, S.-L.; Xie, H.-X.; Zhu, J.; Li, H.; Zhang, X.-S.; Li, J.; Wang, W. *Nat. Commun.* **2011**, *2*, 211.

(2) (a) Mei, T.-S.; Patel, H. H.; Sigman, M. S. *Nature* **2014**, *508*, 340−344. (b) Gong, W.; Zhang, G.; Liu, T.; Giri, R.; Yu, J.-Q. *J. Am. Chem. Soc.* **2014**, *136*, 16940−16946. (c) Zhu, R.-Y.; He, J.; Wang, X.-C.; Yu, J.-Q. *J. Am. Chem. Soc.* **2014**, *136*, 13194−13197. (d) He, J.; Li, S.; Deng, Y.; Fu, H.; Laforteza, B. N.; Spangler, J. E.; Homs, A.; Yu, J.-Q. *Science* **2014**, *343*, 1216−1220. (e) Zaitsev, V. G.; Shabashov, D.; Daugulis, O. *J. Am. Chem. Soc.* **2005**, *127*, 13154−13155. (f) Ano, Y.; Tobisu, M.; Chatani, N. *J. Am. Chem. Soc.* **2011**, *133*, 12984−12986.

(3) (a) Pirnot, M. T.; Rankic, D. A.; Martin, D. B. C.; MacMillan, D. W. C. *Science* **2013**, *339*, 1593−1596. (b) Terrett, J. A.; Clift, M. D.; MacMillan, D. W. C. *J. Am. Chem. Soc.* **2014**, *136*, 6858−6861. (c) Petronijević, F. R.; Nappi, M.; MacMillan, D. W. C. *J. Am. Chem. Soc.* **2013**, *135*, 18323−18326.

(4) (a) Jin, Z.; Chen, S.; Wang, Y.; Zheng, P.; Yang, S.; Chi, Y. R. *Angew. Chem., Int. Ed.* **2014**, *53*, 13506−13509. (b) Fu, Z.; Jiang, K.; Zhu, T.; Torres, J.; Chi, Y. R. *Angew. Chem., Int. Ed.* **2014**, *53*, 6506−6510. (c) Jin, Z.; Jiang, K.; Fu, Z.; Torres, J.; Chen, S.; Zheng, P.; Yang, S.; Song, B.-A.; Chi, Y. R. *Chem. - Eur. J.* **2015**, *21*, 9360−9363.

(5) (a) Maruoka, K.; List, B.; Yamamoto, H.; Gong, L.-Z. *Chem. Commun.* **2012**, *48*, 10703−10703. (b) List, B.; Yang, J. W. *Science* **2006**, *313*, 1584−1586. (c) Mukherjee, S.; Yang, J. W.; Hoffmann, S.; List, B. *Chem. Rev.* **2007**, *107*, 5471−5569. (d) MacMillan, D. W. C. *Nature* **2008**, *455*, 304−308. (e) Bertelsen, S.; Jørgensen, K. A. *Chem. Soc. Rev.* **2009**, *38*, 2178−2189. (f) Dondoni, A.; Massi, A. *Angew. Chem., Int. Ed.* **2008**, *47*, 4638−4660. (g) Barbas, C. F. *Angew. Chem., Int. Ed.* **2008**, *47*, 42−47. (h) Melchiorre, P.; Marigo, M.; Carlone, A.; Bartoli, G. *Angew. Chem., Int. Ed.* **2008**, *47*, 6138−6171. (i) Ryan, S. J.; Candish, L.; Lupton, D. W. *Chem. Soc. Rev.* **2013**, *42*, 4906−4917. (j) Doyle, A. G.; Jacobsen, E. N. *Chem. Rev.* **2007**, *107*, 5713−5743.

(6) (a) Breslow, R. *J. Am. Chem. Soc.* **1958**, *80*, 3719−3726. (b) Arduengo, A. J., III; Harlow, R. L.; Kline, M. *J. Am. Chem. Soc.* **1991**, *113*, 361−363.

(7) (a) Flanigan, D. M.; Romanov-Michaildis, F.; White, N. A.; Rovis, T. *Chem. Rev.* **2015**, DOI: 10.1021/acs.chemrev.5b00060. (b) Bugaut, X.; Glorius, F. *Chem. Soc. Rev.* **2012**, *41*, 3511−3522. (c) Vora, H. M.; Rovis, T. *Aldrichim. Acta* **2011**, *44*, 3−11. (d) Phillips, E. M.; Chan, A.; Scheidt, K. A. *Aldrichim. Acta* **2009**, *42*, 55−66.

(8) (a) Hopkinson, M. N.; Richter, C.; Schedler, M.; Glorius, F. *Nature* **2014**, *510*, 485−496. (b) Nair, V.; Menon, R. S.; Biju, A. T.; Sinu, C. R.; Paul, R. R.; Jose, A.; Sreekumar, V. *Chem. Soc. Rev.* **2011**, *40*, 5336−5346. (c) Yatham, V.; Neudörfl, J.-M.; Schlörer, N. E.; Berkessel, A. *Chem. Sci.* **2015**, *6*, 3706−3711. (d) Berkessel, A.; Yatham, V. R.; Elfert, S.; Neudörfl, J.-M. *Angew. Chem., Int. Ed.* **2013**, *52*, 11158−11162. (e) Ni, Q.; Zhang, H.; Grossmann, A.; Loh, C. C. J.; Merkens, C.; Enders, D. *Angew. Chem., Int. Ed.* **2013**, *52*, 13562−13566. (f) Guo, C.; Schedler, M.; Daniliuc, C. G.; Glorius, F. *Angew. Chem., Int. Ed.* **2014**, *53*, 10232−10236. (g) Lee, A.; Younai, Y.; Price, C. K.; Izquierdo, J.; Mishra, R. K.; Scheidt, K. A. *J. Am. Chem. Soc.* **2014**, *136*, 10589−10592. (h) Kravina, A. G.; Mahatthananchai, J.; Bode, J. W. *Angew. Chem., Int. Ed.* **2012**, *51*, 9433−9436. (i) Zhang, J.; Xing, C.; Tiwari, B.; Chi, Y. R. *J. Am. Chem. Soc.* **2013**, *135*, 8113−8116. (j) Zhu, T.; Zheng, P.; Mou, C.; Yang, S.; Song, B.-A.; Chi, Y. R. *Nat. Commun.* **2014**, *5*, 5027. (k) Candish, L.; Lupton, D. W. *J. Am. Chem. Soc.* **2013**, *135*, 58−61. (l) Han, R.; Qi, J.; Gu, J.; Ma, D.; Xie, X.; She, X. *ACS Catal.* **2013**, *3*, 2705−2709. (m) Yang, L.; Wang, F.; Lee, R.; Lv, Y.; Huang, K.-W.; Zhong, G. *Org. Lett.* **2014**, *16*, 3872−3875. (n) Zhao, M.; Yang, H.; Li, M.-M.; Chen, J.; Zhou, L. *Org. Lett.* **2014**, *16*, 2904−2907. (o) Wang, M. H.; Cohen, D. T.; Schwamb, C. B.; Mishra, R. K.; Scheidt, K. A. *J. Am. Chem. Soc.* **2015**, *137*, 5891−5894. (p) White, N. A.; Rovis, T. *J. Am. Chem. Soc.* **2014**, *136*, 14674−14677.

(9) Fu, Z.; Xu, J.; Zhu, T.; Leong, W. W. Y.; Chi, Y. R. *Nat. Chem.* **2013**, *5*, 835−839.

(10) (a) Reddi, Y.; Sunoj, R. B. *ACS Catal.* **2015**, *5*, 1596−1603. (b) Verma, P.; Verma, P.; Sunoj, R. B. *Org. Biomol. Chem.* **2014**, *12*, 2176−2179. (c) Li, Z.; Wei, D.; Wang, Y.; Zhu, Y.; Tang, M. *J. Org. Chem.* **2014**, *79*, 3069−3078. (d) Johnston, R. C.; Cohen, D. T.; Eichman, C. C.; Scheidt, K. A.; Cheong, P. H.-Y. *Chem. Sci.* **2014**, *5*, 1974−1982. (e) Mahatthananchai, J.; Bode, J. W. *Acc. Chem. Res.* **2014**, *47*, 696−707. (f) Kuniyil, R.; Sunoj, R. B. *Org. Lett.* **2013**, *15*, 5040−5043. (g) Reddi, Y.; Sunoj, R. B. *Org. Lett.* **2012**, *14*, 2810−2813. (h) Allen, S. E.; Mahattananchai, J.; Bode, J. W.; Kozlowski, M. C. *J. Am. Chem. Soc.* **2012**, *134*, 12098−12103. (i) Verma, P.; Patni, P. A.; Sunoj, R. B. *J. Org. Chem.* **2011**, *76*, 5606−5613. (j) Um, J. M.; DiRocco, D. A.; Noey, E. L.; Rovis, T.; Houk, K. N. *J. Am. Chem. Soc.* **2011**, *133*, 11249−11254. (k) Domingo, L. R.; Zaragoza, R. J.; Arno, M. *Org. Biomol. Chem.* **2010**, *8*, 4884−4891.

(11) Grimme, S. *J. Comput. Chem.* **2006**, *27*, 1787−1799.

(12) Zhao, Y.; Truhlar, D. G. *J. Chem. Phys.* **2006**, *125*, 194101−194118.

(13) Grimme, S.; Antony, J.; Ehrlich, S.; Krieg, H. *J. Chem. Phys.* **2010**, *132*, 154104−154123.

(14) (a) Becke, A. D. *Phys. Rev. A: At., Mol., Opt. Phys.* **1988**, *38*, 3098−3100. (b) Becke, A. D. *J. Chem. Phys.* **1993**, *98*, 5648−5652. (c) Lee, C.; Yang, W.; Parr, R. G. *Phys. Rev. B: Condens. Matter Mater. Phys.* **1988**, *37*, 785−789.

(15) Gonzalez, C.; Schlegel, H. B. *J. Phys. Chem.* **1990**, *94*, 5523−5527.

(16) Frisch, M. J.; Trucks, G. W.; Schlegel, H. B.; Scuseria, G. E.; Robb, M. A.; Cheeseman, J. R.; Scalmani, G.; Barone, V.; Mennucci, B.; Petersson, G. A.; Nakatsuji, H.; Caricato, M.; Li, X.; Hratchian, H. P.; Izmaylov, A. F.; Bloino, J.; Zheng, G.; Sonnenberg, J. L.; Hada, M.; Ehara, M.; Toyota, K.; Fukuda, R.; Hasegawa, J.; Ishida, M.; Nakajima, T.; Honda, Y.; Kitao, O.; Nakai, H.; Vreven, T.; Montgomery, J. A., Jr.; Peralta, J. E.; Ogliaro, F.; Bearpark, M.; Heyd, J. J.; Brothers, E.; Kudin, K. N.; Staroverov, V. N.; Kobayashi, R.; Normand, J.; Raghavachari, K.; Rendell, A.; Burant, J. C.; Iyengar, S. S.; Tomasi, J.; Cossi, M.; Rega, N.; Millam, M. J.; Klene, M.; Knox, J. E.; Cross, J. B.; Bakken, V.; Adamo, C.; Jaramillo, J.; Gomperts, R.; Stratmann, R. E.; Yazyev, O.; Austin, A. J.; Cammi, R.; Pomelli, C.; Ochterski, J. W.; Martin, R. L.; Morokuma, K.; Zakrzewski, V. G.; Voth, G. A.; Salvador, P.; Dannenberg, J. J.; Dapprich, S.; Daniels, A. D.; Farkas, Ö.; Foresman, J. B.; Ortiz, J. V.; Cioslowski, J.; Fox, D. J. *Gaussian09, Revision D.01*; Gaussian, Inc.: Wallingford, CT, 2009.

DOI: 10.1021/acscatal.5b01870
ACS Catal. 2015, 5, 5794−5802

(17) Marenich, A. V.; Cramer, C. J.; Truhlar, D. G. *J. Phys. Chem. B* **2009**, *113*, 6378−6396.
(18) (a) *AIM2000 Version 2.0; Buro fur Innovative Software*, SBK-Software, Bielefeld, Germany, 2002. (b) Biegler-Konig, F.; Schonbohm, J.; Bayles, D. *J. Comput. Chem.* **2001**, *22*, 545−559. (c) Biegler-Konig, F.; Schonbohm, J. *J. Comput. Chem.* **2002**, *23*, 1489−1494.
(19) (a) Hong, X.; Liang, Y.; Griffith, A. K.; Lambert, T. H.; Houk, K. N. *Chem. Sci.* **2014**, *5*, 471−475. (b) Jindal, G.; Sunoj, R. B. *Angew. Chem., Int. Ed.* **2014**, *53*, 4432−4435. (c) Bickelhaupt, F. M. *J. Comput. Chem.* **1999**, *20*, 114−128. (d) Diefenbach, A.; Bickelhaupt, F. M. *J. Phys. Chem. A* **2004**, *108*, 8460−8466. (e) Legault, C. Y.; Garcia, Y.; Merlic, C. A.; Houk, K. N. *J. Am. Chem. Soc.* **2007**, *129*, 12664−12665.
(20) (a) Foster, J. P.; Weinhold, F. *J. Am. Chem. Soc.* **1980**, *102*, 7211−7218. (b) Reed, A. E.; Weinhold, F. *J. Chem. Phys.* **1983**, *78*, 4066−4073. (c) Reed, A. E.; Weinstock, R. B.; Weinhold, F. *J. Chem. Phys.* **1985**, *83*, 735−746.
(21) The forward IRC of this transition state and subsequent geometry optimization starting from the end points of IRC runs show that the phenoxide leaves the carbonyl carbon, as is evident from an increase in the C−O bond distance from 1.92 to 2.41 Å.
(22) (a) An alternative pathway wherein DBU abstracts the α-C−H proton of intermediate **3** is found to be 11.9 kcal/mol higher in energy. (b) See Scheme S1 and Figure S3 in the Supporting Information.
(23) Additional details are provided in Scheme S2 and Figure S4 in the Supporting Information.
(24) The natural population analysis indicates that the β-C−H protons in intermediate **5** are more acidic than those in the parent compound **1** as well as those in the intermediate **4**. See Figure S5 in the Supporting Information for additional details and comparison.
(25) A comparative energy profile diagram as well as that of the formation of a β-lactam product is provided in Figure S10 and Scheme S4 in the Supporting Information.
(26) The optimized geometries of the transition state are given in Figure S1 in the Supporting Information.
(27) Additional details such as the optimized geometries are provided in Figure S1 in the Supporting Information.
(28) The transition state could not be located even after repeated attempts. Problems such as methyl rotation (methyl of the *tert*-butyl group) as well as collapse to the reactant/product has been noticed. Changing the integration grid to *ultrafine* as well as the use of quasi-Newton synchronous transit methods for transition state optimization all failed to locate this elusive stationary point in the condensed phase.
(29) (a) The enolate $\mathbf{5}_{\mathbf{PhOH}}$ can be obtained either along the IRC trajectory of **TS(4-5)** in the forward direction or through that of $\mathbf{TS(5\text{-}6)}_{\mathbf{PhOH}}$ in the reverse direction. The lower energy conformer of $\mathbf{5}_{\mathbf{PhOH}}$ is shown in Figure 1. (b) The energy difference between these two conformers of $\mathbf{5}_{\mathbf{PhOH}}$ is about 6 kcal/mol.
(30) Details of the IRC profile, geometric features, and Wiberg bond indices along the IRC trajectory are provided respectively in Figure S8 and Table S1 in the Supporting Information.
(31) (a) IRC paths on either side of the transition state revealed that the enolate O−H distance in **6** (0.97 Å) progressively increases as it gets closer to the transition state (**TS(6-7)** 1.02 Å) and then further toward the product side (1.46 Å), as noted at the end point of the IRC trajectory. (b) Additional details on the IRC trajectory, bond distances, and Wiberg bond indices are provided respectively in Figure S14 and Table S7 in the Supporting Information.
(32) IRC calculations clearly indicated that the processes of C−C bond formation and the proton transfer are concerted. See Figure S14 in the Supporting Information.
(33) (a) Knowles, R. R.; Jacobsen, E. N. *Proc. Natl. Acad. Sci. U. S. A.* **2010**, *107*, 20678−20685. (b) Wheeler, S. E.; Bloom, J. W. G. *J. Phys. Chem. A* **2014**, *118*, 6133−6147. (c) Uyeda, C.; Jacobsen, E. N. *J. Am. Chem. Soc.* **2011**, *133*, 5062−5075.
(34) See Figure S13 in the Supporting Information for a plot of the bond paths and the bond critical points.
(35) Various experimental and theoretical studies have been carried out to understand the nature of these interactions. On the basis of these studies cutoff values for these interactions are generally H···x1(x2) distance <3.2 Å and angle CHx1(x2) > 120° or HCx1(x2) < 60°. (a) Nishio, M.; Umezawa, Y.; Hirota, M.; Takeuchi, Y. *Tetrahedron* **1995**, *51*, 8665−8701. (b) Umezawa, Y.; Tsuboyama, S.; Takahashi, H.; Uzawa, J.; Nishio, M. *Tetrahedron* **1999**, *55*, 10047−10056. (c) Takahashi, H.; Tsuboyama, S.; Umezawa, Y.; Honda, K.; Nishio, M. *Tetrahedron* **2000**, *56*, 6185−6191.
(36) (a) Additional analyses using the activation strain model revealed a slightly lower distortion of the reacting partners in the lower energy *si,re* transition state. (b) For more details see page S22 in the Supporting Information.
(37) See Figures S11 and S12 and Table S4 in the Supporting Information for all the possible modes for the stereochemical C−C bond formation transition states, optimized geometries, and corresponding energies.
(38) We could not locate this transition state even after several attempts.
(39) Full details of the Hammett analysis are provided in Figure S16 in the Supporting Information.

DOI: 10.1021/acscatal.5b01870
ACS Catal. 2015, 5, 5794−5802